



ELSEVIER

Available online at www.sciencedirect.com

ScienceDirect

journal homepage: www.elsevier.com/locate/he

CFD-driven surrogate-based multi-objective shape optimization of an elbow type draft tube

Gizem Demirel ^a, Erdem Acar ^a, Kutay Celebioglu ^b, Selin Aradag ^{a,b,*}

^a TOBB University of Economics and Technology, Department of Mechanical Engineering, Sogutozu Avenue 43, Sogutozu, Ankara, 06560, Turkey

^b TOBB University of Economics and Technology, Hydro Energy Research Lab (ETU Hydro), Sogutozu Avenue 43, Sogutozu, Ankara, 06560, Turkey

ARTICLE INFO

Article history:

Received 14 October 2016

Received in revised form

25 February 2017

Accepted 11 March 2017

Available online 2 April 2017

Keywords:

Francis turbine

Draft tube

Optimization

Pressure recovery factor

Meta-model

ABSTRACT

Draft tube is the part of Francis turbines which is used to both discharge water and recover kinetic energy at the exit of the runner. A design optimization study of an elbow type draft tube based on the combined use of Computational Fluid Dynamics (CFD), design of experiments, surrogate models and multi-objective optimization is presented in this study. The geometric variables that specify the shape of the draft tube are chosen as input variables for surrogate models and the pressure recovery factor and the head loss are selected as output responses. It is determined that, pressure recovery factor, which is the main performance parameter, can be increased by 4.3%, and head loss can be reduced by %20 compared to the initial CFD aided design. Pressure recovery factor, is represented with a second order polynomial regression model in terms of the geometrical parameters based on the optimization results. The verification of the model is also provided by comparison with CFD results for different draft tubes other than that are used in the development of the model. The model is verified using 30 different design points and it can predict the pressure recovery factor with an error of less than 8%. This model allows the fast and correct design and optimization of elbow type draft tubes, without the need for further CFD simulations.

© 2017 Hydrogen Energy Publications LLC. Published by Elsevier Ltd. All rights reserved.

Introduction

Hydro energy is one of the most sustainable, reliable, and cost-effective form of energy. The advantages of hydro energy over other renewable energy sources are that it emits limited amounts of greenhouse gases, is very cost-effective, and the amount produced can be tailored to meet consumer demands [1]. Francis, Kaplan and Pelton are the most commonly used water turbines, and amongst these types the Francis turbine is

the most preferred one due to its larger range of flow rate and head values.

A Francis type turbine consists of three main parts. These are the runner, where energy is produced, the spiral case, stay vanes and guide vanes that transfer water from the turbine inlet to runner, and the draft tube which discharges water from runner to tail water. Draft tube is used to both discharge water and recover kinetic energy at the exit of the runner producing vacuum. Pressure recovery and head loss from inlet

* Corresponding author. TOBB University of Economics and Technology, Department of Mechanical Engineering, Sogutozu Avenue 43, Sogutozu, Ankara, 06560, Turkey.

E-mail address: saradag@etu.edu.tr (S. Aradag).

<http://dx.doi.org/10.1016/j.ijhydene.2017.03.082>

0360-3199/© 2017 Hydrogen Energy Publications LLC. Published by Elsevier Ltd. All rights reserved.

to outlet of a draft tube are generally used to determine the effectiveness of this component [2,3].

An elbow type draft tube comprises three main parts: cone, elbow and diffuser. Cross-sectional area is increased to reduce the velocity and kinetic energy of water along the draft tube cone and diffuser. However, the area of the elbow part is usually kept constant to reduce frictional losses. Although conventional hydro turbine design practice is based on experience, use of modern optimization techniques can result in better solutions.

Computational Fluid Dynamics (CFD) became a powerful tool in the design and analysis of turbomachinery recently. Modeling of hydroturbines proved to be useful in design [4]. Especially, the reasons of loss of performance can be determined more easily compared to model tests [5]. Although turbulent, three dimensional Navier–Stokes simulations are time consuming, even one dimensional CFD analysis for draft tubes can be useful to determine the effects of design parameters on performance [6].

Different optimization techniques have been used in design and rehabilitation of hydraulic turbines for the last decades [7]. Discrete algorithms, evolutionary algorithms and algorithms based on the direction of search (gradient based local search or global search) that are incorporated with CFD, have widely been used to determine optimum shapes for turbine components. However, the fact that which algorithm is better for what kind of application is still not clear [8–10]. The optimization process also requires a large amount of computational time and effort.

Design of experiments step is an important part of surrogate-based optimization where the design points that directly affect the accuracy of the surrogate models are determined. For simulation based studies, Latin hypercube sampling, optimal space filling, sparse grid initialization are some of the methods used in literature [11]. For experimental studies, on the other hand, factorial experimental designs are preferred [12,13]. If time-variant design variables exist, then design of dynamic experiments technique can also be used [14].

After the design points (i.e., training points) are determined, response values are computed at the design points and the surrogate models are constructed to relate responses to the design variables. The standard second order polynomial response surface, Kriging, nonparametric regression and neural network are amongst the most commonly used surrogate model types in literature [11].

An automated optimization methodology is necessary for draft tubes in order to obtain a quick optimized design. Ayancik et al. [11] used several of these methods for the optimization of the runner of a Francis turbine, since it is not known a priori which of the methods would provide better results. Acar et al. [15] found out that the optimum that is determined using a method which provides the most accurate result does not guarantee an optimum design with best performance.

In this article, firstly, design optimization study of an elbow type draft tube, based on the combined use of design of

experiments, surrogate models and multi-objective optimization is presented. The use of this surrogate based approach alleviates the computational cost. Computational fluid dynamics (CFD) is also integrated to the optimization process. Pressure recovery factor, which is the main performance parameter, is represented with a regression equation in terms of the geometrical parameters based on the optimization results. Such a model allows the fast and correct design and optimization of elbow type draft tubes, without the need for CFD simulations. The verification of the regression model is also provided by comparison with CFD results for different draft tubes other than that are used in the development of the model.

CFD-Driven Surrogate-Based Design Optimization methodology

The design geometry can be automatically generated and modified with an optimization system. In any optimization process, design variables, objective and constraints should be specified and written in a standard form as in Equation (1) [16,17].

$$\begin{aligned} &\text{Find } \mathbf{x} = \{x_1, x_2, \dots, x_n\} \\ &\text{Min } f(\mathbf{x}) \\ &\text{S.t. } h_j(\mathbf{x}) = 0, \quad j = 1, \dots, n_e \\ &\quad g_k(\mathbf{x}) \leq 0, \quad k = 1, \dots, n_g \\ &\quad \mathbf{x}^L \leq \mathbf{x} \leq \mathbf{x}^U \end{aligned} \quad (1)$$

where \mathbf{x} is a vector representing the design variables, f is the objective function, h and g are the equality and inequality constraints, \mathbf{x}^L and \mathbf{x}^U are the lower and upper bounds of the design variables.

The flowchart used for the design and optimization of the draft tube is tabulated in Fig. 1. It starts with the parameterization of the tube. The shape is represented by a number of parameters. Initial simulation should be prepared by the user for parameter selection. After the manual initiation, automatic optimization process starts. After selecting the shape parameters and upper and lower limits of these parameters, CFD simulations are performed in the range of limits based on Design of Experiment (DoE) method. Response surface models (i.e., surrogate models, metamodels) are used to estimate an approximate model for output parameters in terms of design parameters. Finally, the multi-objective optimization algorithms are used to find the optimum solution by using the response surface models [18].

Parameterization

Parameterization makes it easy to regenerate the design, mesh, perform CFD analysis and post-processing. Five independent geometrical parameters are selected as design variables: cone angle (θ_1), cone height (H_1), elbow radius (R), diffuser angle (θ_2) and diffuser length (H_2) (Fig. 2), in order to define the geometry. Pressure recovery factor (C_p) and head



Fig. 1 – Optimization flow chart.

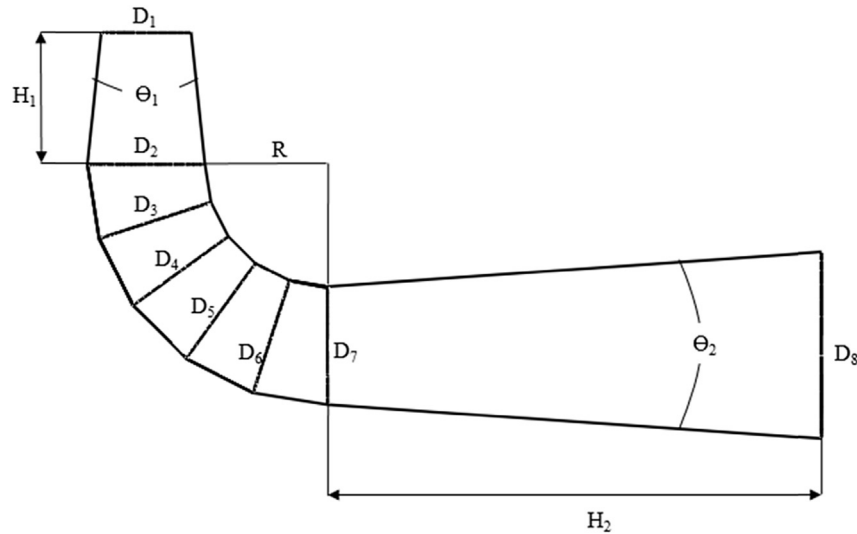


Fig. 2 – Draft tube shape parameters.

loss (ΔH), are used as output parameters of the optimization system as given in Equation (2) and Equation (3) to measure the effectiveness. These output responses are obtained from the CFD analysis.

$$C_p = \frac{P_{out,s} - P_{in,s}}{1/2\rho V_{in}^2} \quad (2)$$

$$\Delta H = \frac{P_{out,t} - P_{in,t}}{\rho g} \quad (3)$$

where $P_{out,s}$ is the static pressure at the draft tube exit, $P_{in,s}$ is the static pressure at the draft tube inlet, $P_{out,t}$ is the total pressure at the draft tube exit, $P_{in,t}$ is the total pressure at the draft tube inlet, ρ is the density of water and V_{in} is the velocity at the draft tube inlet [9].

The multi-objective design optimization of the draft tube can be formulated as given in Equation (4). Since a typical acceptable design for the draft tube has a pressure recovery factor between 0.8 and 0.85, the pressure recovery factor is defined as greater than 0.8 as a constraint for the optimization. The geometric limits used for the process are also shown in the equation.

$$\begin{aligned} \text{Find } & \theta_1, \theta_2, H_1, H_2, R \\ \text{Min } & -C_p, \Delta H \\ \text{S.t. } & 0.8 - C_p \leq 0 \\ & 5 \leq \theta_1 \leq 15 \\ & 720 \leq H_1 \leq 1000 \\ & 990 \leq R \leq 1400 \\ & 5 \leq \theta_2 \leq 15 \\ & 2700 \leq H_2 \leq 3500 \end{aligned} \quad (4)$$

The properties of the baseline design used for optimization is presented in Table 1. It is determined with CFD analysis. Several researchers in the field of design and optimization of hydraulic turbines performed their studies with the help of CFD techniques. In this work, the methodology used and developed by our group [19,20] is utilized for the CFD analysis. Flow simulations are carried out per this methodology by using the commercial software ANSYS 16.0 [21] based on

steady state Reynolds-Averaged Navier–Stokes equations using k- ϵ turbulence model (medium intensity).

CFD analysis and computational details

Three dimensional turbulent Reynolds Averaged Navier–Stokes (RANS) equations are solved in the CFD analysis for incompressible flow using k- ϵ turbulence model, where k is the turbulent kinetic energy and ϵ is turbulent kinetic energy dissipation. The number of grid points are 3.5 million to satisfy mesh independence. The domain is meshed with unstructured grids using triangular and tetrahedral elements. The computations are performed using an HP Z-840 workstation utilizing parallel computations of 30 processors. The

Table 1 – Properties of the baseline design.

Geometrical parameter	Value	Variable type
D1	530 mm	Independent
D2	698,1 mm	Dependent
D3	698,1 mm	Dependent [D2] $D3 = D1 + 2*H1*\tan\left(\frac{\theta_1}{2}\right)$
D4	698,1 mm	Dependent [D2] $D4 = D2$
D5	698,1 mm	Dependent [D2] $D5 = D2$
D6	698,1 mm	Dependent [D2] $D6 = D2$
D7	698,1 mm	Dependent [D2] $D7 = D2$
D8	1117,7 mm	Dependent $D8 = D2 + 2*H2*\tan\left(\frac{\theta_2}{2}\right)$
H1	800 mm	Independent
H2	3000 mm	Independent
R1	1100 mm	Independent
θ_1	12°	Independent
θ_2	8°	Independent

computation time for one draft tube simulation is three hours with 30 processors.

The geometry is imported and geometric parameters are selected as input parameters. At the design point, runner outflow swirl is nearly zero to increase power output; therefore, fluid enters the tube vertically (normal to the boundary) and mass flow inlet ($2 \text{ m}^3/\text{s}$) boundary condition is selected. For outlet boundary condition, pressure outlet is given as atmospheric pressure (1 atm). No backflow is allowed. All other parts are considered as wall with no slip condition. The analysis is performed using CFX module [21] and grid topology and flow properties are kept unchanged for all the analyses. Information in Ayli et al. [20] is used to obtain a mesh independent solution.

Design of Experiment (DoE)

The optimization process starts with generating the sampling space within the lower and upper limits. Locations of the sample points in design space affect the accuracy of the response surface, so choosing an effective DoE method becomes significant. In order to determine the distribution of sampling points, two DoE methods are selected: Custom Sampling (CS) and Latin Hypercube Sampling (LHS). The advantage of these methods is that the number of sample points can be selected manually which affects both quality of prediction and randomness of the response surface. In this study, 50 data points (i.e., training points), are generated for each DoE type. The number of data points is chosen to be ten times the number of design variables.

Surrogate modeling

Once the DoE is generated and results are obtained, an approximate model (i.e., a surrogate model) is constructed for each output variable in terms of the input design variables. There is a gap in literature about selection of the most accurate type of surrogate model to be used for elbow type draft tube optimization, so several different surrogate models are constructed: namely, the standard second order polynomial response surface, Kriging, nonparametric regression and neural network. In order to assess the accuracy of these surrogate models, 10 test points are generated. The results are shown in Table 2. It is observed that the constructed surrogate models have acceptable accuracy (relative Root Mean Square Error, RMSE values are smaller than 5%), and the standard second order polynomial model is the most accurate when the error metric of our interest is the relative RMSE.

Table 2 – Accuracies of the constructed surrogate models.

Surrogate model	Relative RMSE (%)	
	Cp	ΔH
Standard second order polynomial response surface	0.07	0.45
Kriging	0.06	0.50
Nonparametric regression	0.56	4.86
Neural network	0.11	0.75

Multi-objective optimization

Two different search algorithms are used in optimization; screening and multi-objective genetic algorithm (MOGA) which can handle multiple objective functions. The working principle of the screening method is direct sampling by a quasi-random number generator based on the Hammersley algorithm and then sorting the samples based on objectives and constraints. The other method, MOGA, provides a more refined approach than the screening method with an iterative approach.

In optimization, maximization of recovery factor and minimization of head loss are selected as objective functions and one constraint function is set to the recovery factor values that should be greater than or equal to 0.8. After the optimization problem is solved by using surrogate models, the final step is to verify the optimization results by conducting CFD analysis of the optimum design.

Results and discussion

In this section, firstly, the results of CFD-Driven Surrogate-Based Design Optimization will be presented and discussed in detail in Section [CFD-Driven Surrogate-Based Design Optimization Results](#). Then, the pressure recovery factor is represented with a regression equation in terms of the geometrical parameters based on the optimization results. The results of this part are summarized in section [Development of a Regression Equation for draft tube performance prediction with the help of the results of the optimization study](#). Finally, the verification of the regression model is provided by comparison with CFD results for different draft tubes other than that are used in the development of the model. These results are presented and discussed in section [Verification of the developed regression equations](#).

CFD-Driven Surrogate-Based Design Optimization results

Draft tube designs are performed in Ansys Workbench by using CFX (Fluid Flow), and Response Surface Optimization modules [21]. Input and output variables are defined in the parameter set. Optimization process includes geometry optimization to reach maximum pressure recovery factor with minimum head loss. Since four different surrogate models and two different optimizers are used, eight candidate optimum designs are generated (Table 3). It is seen that the optimum candidate design achieved by using standard second order polynomial response surface surrogate model and MOGA optimization algorithm displays the best performance, so it is taken as the optimum design.

An existing draft tube is taken from an actual power plant which has % 92.8 overall turbine efficiency. The recovery factor of the baseline draft tube design is 0.813 which is assumed to be very efficient according to the literature [3]. The properties of the initial and the optimized designs are shown in Table 4. It is seen that the optimum design has 0.848 pressure recovery factor (increased by 4.3% compared to the initial design) and 0.448 m head loss (reduced by 20% compared to the initial design).

Table 3 – Eight candidate optimum designs.

#	Surrogate model	Optimizer	θ_1 [°]	θ_2 [°]	H1 [mm]	H2 [mm]	R [mm]	Cp	ΔH [m]
1	KR ^a	MOGA	10.86	7.37	954	3277	1377	0.841	0.451
2	KR	Screening	11.27	7.52	998	3324	1340	0.839	0.481
3	NPR ^a	MOGA	11.36	7.81	931	3144	1326	0.840	0.473
4	NPR	Screening	11.26	7.92	928	3173	1233	0.838	0.480
5	NN ^a	MOGA	10.97	7.24	980	3176	1361	0.841	0.479
6	NN	Screening	11.27	7.52	998	3324	1340	0.832	0.485
7	RS ^a	MOGA	10.80	7.27	994	3455	1399	0.848	0.448
8	RS	Screening	10.80	8.81	983	3300	1397	0.844	0.450

Bold values indicate the selected optimum design.

^a KR: Kriging, NPR: Non-parametric regression, NN: neural network, RS: response surface.

Table 4 – Comparison of initial and optimized designs.

	Initial Design	Optimized Design
Cone Angle [°]	12.00	10.80
Cone Height [mm]	800	994
Elbow Radius [mm]	1100	1399
Diffuser Angle [°]	8.00	7.27
Diffuser Length [mm]	3000	3455
Pressure Recovery Factor [-]	0.813	0.848
Head Loss [m]	0.560	0.448

Fig. 3 shows the pressure distribution on the midplane of the initial and optimized draft tubes. Fig. 4 shows the streamlines for the optimized case. The CFD results for the optimum design show that the static pressure increases up to the atmospheric pressure along the draft tube because of the reduction of velocity (nearly zero) and kinetic energy which are acceptable per Bernoulli equation if the potential energy change is ignored. The flow attaches to the draft tube walls that makes boundary layer detachment and occurrence of backflow harder and reduces the losses caused by friction.

To examine the effects of the elbow part on the flow, velocity vectors in the mid plane and velocity streamlines along the draft tube are examined where the flow slowed down and where flow separation takes place. Both tangential velocity component of the fluid at inlet and the elbow of the draft tube cause flow separation and backflow which cause vortices in and after the elbow part of the draft tube. Flow separation and formation of vortices can be prevented by adjusting the inclination of the draft tube cone. If the angle is increased too much, reverse pressure gradients occur. However, if the inclination is not enough, velocity of the fluid will not decrease and flow will enter the elbow part with high

velocities increasing the friction losses. Figs. 3b and 4b show that no separation occurs along the draft tube. However, sudden velocity reduction at the elbow part corners cause the pressure increase and friction losses. So, increase in cross sectional areas should be distributed carefully considering the cone and diffuser angles and the transition between them should be smooth.

A sensitivity analysis is also performed to investigate the impact of the design variables on the output responses. For each output, the weights of different design parameters are presented in Table 5. It is seen that angles of cone (θ_1) and diffuser (θ_2) are the most significant design variables that affect the pressure recovery factor and the head loss.

It is possible to change the cone and diffuser angles to prevent hydraulic losses arising from vortices and separation. Reverse pressure gradients occur if the cone angle increases more than enough. If it is smaller than necessary, the velocity of the flow does not decrease enough, causing the fluid to enter the elbow with high velocities, which increases friction losses. The optimum cone angle is computed to be 11° to maximize the pressure recovery factor and 9° to minimize the losses. The effects of diffuser angle on the results is such that both pressure recovery factor and head loss increase up to 11° , pressure factor decreases sharply after this angle whereas the losses continue increasing.

Cone height (H1), elbow radius (R), and diffuser length (H2) are also other factors that cause an increase in pressure recovery factor, per the computational results. The head loss also increases with diffuser length, whereas an increase in the other two parameters helps to decrease the head losses. Head loss remains the same after a certain cone height and diffuser length. (For this case, they are 930 mm and 3200 mm, resulting in a head loss of 0.52.)

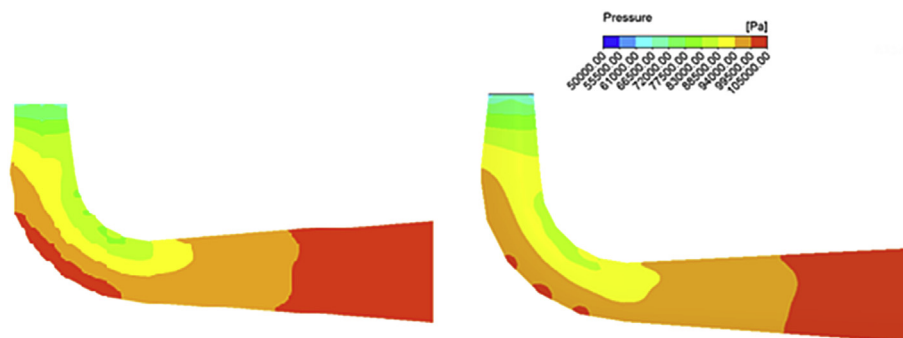


Fig. 3 – Pressure distribution on the (a) Initial (b) optimized draft tube mid plane.

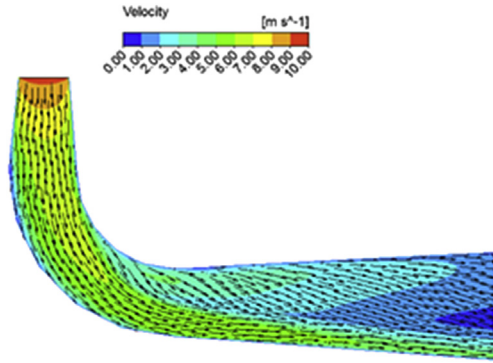


Fig. 4 – Streamlines on the draft tube midplane of the optimized design.

Table 5 – Sensitivities of parameters for (a) pressure recovery factor (b) head loss.

Effect on:	Pressure recovery factor (%)	Head loss (%)
Theta 1	45	40
Theta 2	25	45
H1	6	5
H2	11	4
R1	12	6

Horhersall [22] increases the length of the diffuser to increase the surface area for water to leave the draft tube and to decrease the kinetic energy losses. However, increasing this length causes separation in the flow, resulting in more losses as seen in Fig. 5.

Fig. 6 presents the Pareto front that shows the relation between the objective functions: pressure recovery factor and head loss. As pressure recovery factor increases, head loss also increases.

Development of a regression equation for draft tube performance prediction with the help of the results of the optimization study

It is important to show the performance of a draft tube in the optimization process with a function instead of using computational fluid dynamics as a part of the optimization process. Therefore, CFD is first used to generate data for a regression analysis and once a regression model is developed, the model is used to predict the pressure recovery factor in the optimization process. Table 6 shows the parameters that affect the pressure recovery factor of the draft tube.

Eleven different variables are used to define the system. As a representative figure to show the dependance of Pressure recovery factor on these parameters, Fig. 7 is presented.

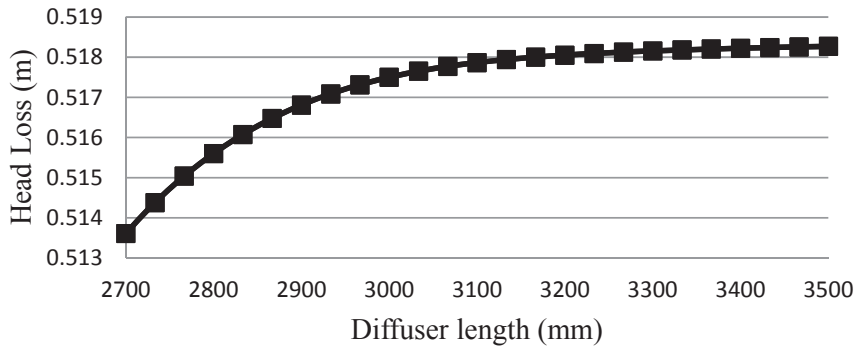


Fig. 5 – Effect of diffuser length on head loss.

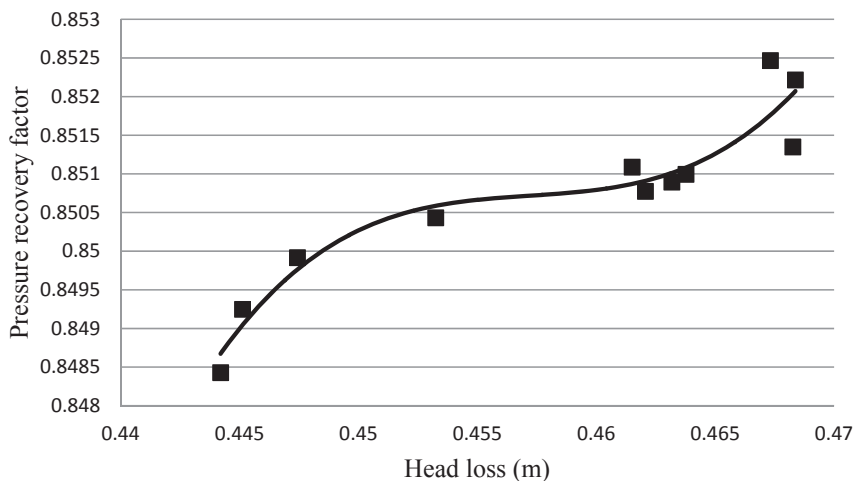
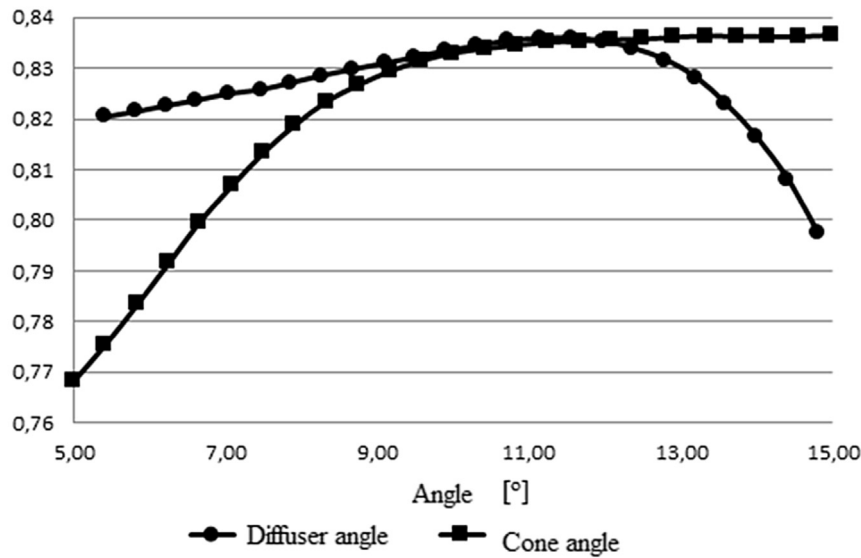


Fig. 6 – Pareto front for the objective functions.

Table 6 – Parameters that affect the pressure recovery factor.

Variable	Symbol	Definition	Unit
Dependent	ΔP	Pressure difference	[Nm ²]
Independent	D_2	Draft tube inlet diameter	[m]
	H_1	The length of the conical part	[m]
	θ_1	Cone angle	[°]
	H_2	Diffuser length	[m]
	θ_2	Diffuser angle	[°]
	R	Elbow radius	[m]
	V	Velocity at the draft tube inlet	[ms ⁻¹]
	μ	Dynamic viscosity	[Nm ⁻² s]
	ρ	Density	[Nm ⁻⁴ s ²]
	ϵ	Surface roughness	[m]

Pressure recovery factor**Fig. 7 – Dependance on pressure recovery factor on diffuser and cone angles.**

Using dimensional analysis and Buckingham-Pi theorem, the pressure recovery factor is obtained as a function of non-dimensional variables formed using the dependent and independent variables in Table 5.

$$C_p = \frac{P_{out} - P_{in}}{\frac{1}{2}\rho V^2} = f\left(\frac{H_1}{D_2}, \frac{H_2}{D_2}, \frac{R}{D_2}, \theta_1, \theta_2, Re, \frac{\epsilon}{D_2}\right)$$

The limits for the determined non dimensional parameters are determined based on the work by Gubin [18] are shown in Table 7. CFD analyses are performed for seventy different design points and the values of all the non-

Table 7 – Limits of the regression model.

Non-dimensional parameter	Lower limit	Upper limit
$\frac{H_1}{D_2}$	0,8	2,5
$\frac{H_2}{D_2}$	3	9,5
$\frac{R}{D_2}$	1	3,5
θ_1	5	15
θ_2	5	15
Re	10^6	10^7
$\frac{\epsilon}{D_2}$	10^{-5}	10^{-4}

dimensional parameters for the data points are obtained with the help of CFD.

Two different regression models are formed. The difference between these two, the sixth and the seventh parameters as shown in Table 8. In one of the models, the logarithm of the Reynolds number and non-dimensionalized surface roughness are used, whereas these parameters are used directly in the other regression model.

In this study, quadratic regression models are used, and the regression model parameters are computed using the method of ordinary least squares [23]. Meta-heuristic methods such as particle swarm optimization [24] were also used in literature to determine regression model parameters [25]. The regression equations obtained for the pressure recovery factor from the first and second regression models are shown in Annex.

Verification of the developed regression equations

It is necessary to validate the developed regression models for the design of different draft tubes. 30 random design points are generated and simulated with CFD to be able to verify the developed regression models. Fig. 8 shows the comparison of

Table 8 – Regression models.

X_i	X_1	X_2	X_3	X_4	X_5	X_6	X_7	
Non-dimensional parameter	Regression model 1	$\frac{H_1}{D_2}$	$\frac{H_2}{D_2}$	$\frac{R}{D_2}$	θ_1	θ_2	Re	$\frac{e}{D_2}$
	Regression model 2	$\frac{H_1}{D_2}$	$\frac{H_2}{D_2}$	$\frac{R}{D_2}$	θ_1	θ_2	$\log(\text{Re})$	$\log\left(\frac{e}{D_2}\right)$

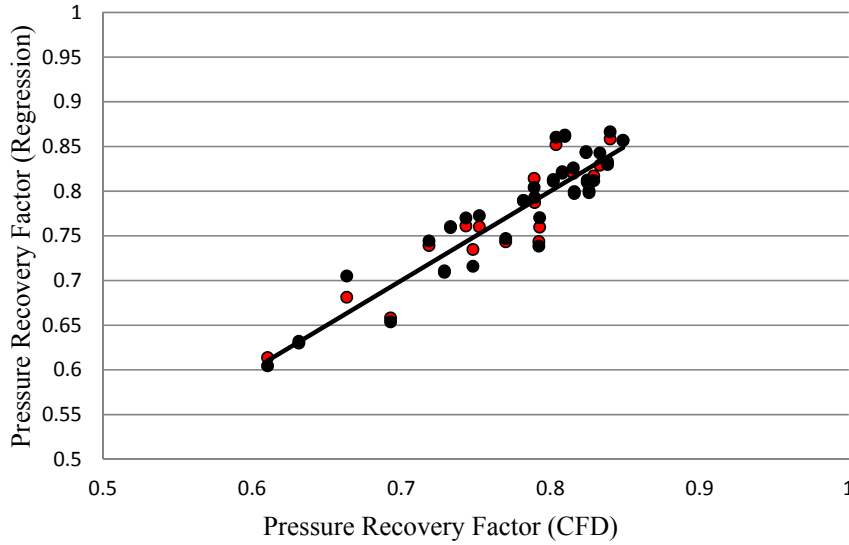


Fig. 8 – Predicted pressure recovery factor versus CFD results (red: regression model 1, black: regression model 2). (For interpretation of the references to colour in this figure legend, the reader is referred to the web version of this article.)

the pressure recovery factors calculated using the CFD results and the ones predicted using the regression models for the test points.

Table 9 shows the errors associated with the regression models. The error definitions are given by:

$$\text{Maximum percentage absolute error} = \max_{i=1, \dots, N} \left\{ \frac{|y_i - \hat{y}_i|}{y_i} * 100 \right\} \tag{5}$$

$$\text{RMSE}_n = \sqrt{\frac{1}{N} \sum_{i=1}^N \left(\frac{y_i - \hat{y}_i}{y_i} \right)^2}, \quad i = 1, \dots, N \tag{6}$$

$$\text{MAE}_n = \frac{1}{N} \sum_{i=1}^N \left| \frac{y_i - \hat{y}_i}{y_i} \right|, \quad i = 1, \dots, N \tag{7}$$

Table 9 – Errors of the regression models.

	Regression model 1		Regression model 2	
	At data points	At test points	At data points	At test points
Max absolute error [%]	7,9	6,6	7,9	7,0
RMSE	0,025	0,039	0,025	0,038
MAE	0,019	0,044	0,019	0,044

Here N is the number of design points, y_i is the CFD result at point i and \hat{y}_i is the prediction of the regression model at point i.

As shown both in Table 9 and Fig. 8, the errors of the regression models are below 8 percent. Therefore, the models can definitely be used in the optimization process of draft tubes with geometrical parameters in the defined range, instead of CFD simulations. This model allows the fast and correct design and optimization of elbow type draft tubes, without the need for CFD simulations.

Conclusions

An optimization design study of an elbow type draft tube based on the combined use of Computational fluid dynamics (CFD), design of experiments, surrogate models and multi-objective optimization is presented in this study. The geometric variables that specify the shape of the draft tube are chosen as input variables for surrogate models and the pressure recovery factor and the head loss are selected as output responses. It is found that, pressure recovery factor, which is the main performance parameter, can be increased by 4.3%, and head loss can be reduced by %20 reduction compared to the initial CFD aided design.

Pressure recovery factor, is represented with a second order polynomial regression model in terms of the geometrical parameters based on the optimization results. The verification of the model is also provided by comparison with CFD

results for different draft tubes other than that are used in the development of the model. The model is verified using 30 different design points and it can predict the pressure recovery factor with an error of less than 8%. This model allows the fast and correct design and optimization of elbow type draft tubes, without the need for further CFD simulations where the computation time for each draft tube analysis is three hours per draft tube with 30 processors. However, using the regression model takes only a few seconds.

Acknowledgments

The computations are performed using the computational cluster and computer infrastructure of TOBB ETU Hydro Energy Research Laboratory, financially supported by Turkish Ministry of Development. The first author was also financially supported by Turkish Scientific and Research Council (Tubitak) BIDEB program for her MS studies which is the subject of this article.

Annex

$$\begin{aligned}
 C_p = & -2,64804 \cdot 10^{-1} + 2,59210 \cdot 10^{-1} \cdot \frac{H_1}{D_2} + 6,08059 \cdot 10^{-2} \cdot \frac{H_2}{D_2} \\
 & + 1,81588 \\
 & \cdot 10^{-1} \cdot \frac{R}{D_2} + 6,52905 \cdot 10^{-2} \cdot \theta_1 - 6,94084 \cdot 10^{-4} \cdot \theta_2 + 7,85441 \\
 & \cdot 10^{-9} \cdot \text{Re} - 1,40116 \cdot 10^{+3} \cdot \frac{\varepsilon}{D_2} + 7,91587 \cdot 10^{-4} \cdot \frac{H_1 H_2}{D_2 D_2} \\
 & - 1,22405 \cdot 10^{-2} \cdot \frac{H_1 R}{D_2 D_2} - 1,33463 \cdot 10^{-2} \cdot \frac{H_1 \theta_1}{D_2} + 9,67152 \\
 & \cdot 10^{-3} \cdot \frac{H_1 \theta_2}{D_2} + 3,63762 \cdot 10^{-9} \cdot \frac{H_1}{D_2} \cdot \text{Re} + 2,58107 \cdot 10^{+1} \cdot \frac{H_1 \varepsilon}{D_2 D_2} \\
 & - 2,40994 \cdot 10^{-3} \cdot \frac{H_2 R}{D_2 D_2} - 1,73122 \cdot 10^{-3} \cdot \frac{H_2 \theta_1}{D_2} - 2,81949 \\
 & \cdot 10^{-3} \cdot \frac{H_2 \theta_2}{D_2} - 5,99250 \cdot 10^{-10} \cdot \frac{H_2}{D_2} \cdot \text{Re} + 2,73720 \cdot 10^{+1} \\
 & \cdot \frac{H_2 \varepsilon}{D_2 D_2} - 2,79582 \cdot 10^{-3} \cdot \frac{R}{D_2} \cdot \theta_1 + 6,08363 \cdot 10^{-3} \cdot \frac{R}{D_2} \cdot \theta_2 \\
 & + 2,62219 \cdot 10^{-9} \cdot \frac{R}{D_2} \cdot \text{Re} - 2,42891 \cdot \frac{R \varepsilon}{D_2 D_2} + 2,66191 \cdot 10^{-3} \\
 & \cdot \theta_1 \theta_2 - 6,50755 \cdot 10^{-10} \cdot \theta_1 \cdot \text{Re} + 1,14566 \cdot 10^{+1} \cdot \theta_1 \cdot \frac{\varepsilon}{D_2} \\
 & - 4,14693 \cdot 10^{-10} \cdot \theta_2 \cdot \text{Re} - 5,93925 \cdot 10^{+1} \cdot \theta_2 \cdot \frac{\varepsilon}{D_2} + 3,39593 \\
 & \cdot 10^{-5} \cdot \text{Re} \cdot \frac{\varepsilon}{D_2} - 4,44130 \cdot 10^{-2} \cdot \left(\frac{H_1}{D_2}\right)^2 + 4,69054 \cdot 10^{-5} \\
 & \cdot \left(\frac{H_2}{D_2}\right)^2 - 3,27520 \cdot 10^{-2} \cdot \left(\frac{R}{D_2}\right)^2 - 1,89007 \cdot 10^{-3} \cdot (\theta_1)^2 \\
 & - 1,99237 \cdot 10^{-3} \cdot (\theta_2)^2 - 5,01090 \cdot 10^{-16} \cdot (\text{Re})^2 + 9,78194 \\
 & \cdot 10^{+6} \cdot \left(\frac{\varepsilon}{D_2}\right)^2
 \end{aligned} \tag{5}$$

$$\begin{aligned}
 C_p = & -4,34644 + 1,13194 \cdot 10^{-1} \cdot \frac{H_1}{D_2} + 1,32560 \cdot 10^{-1} \cdot \frac{H_2}{D_2} \\
 & - 1,45048 \cdot 10^{-3} \\
 & \cdot \frac{R}{D_2} + 9,47621 \cdot 10^{-2} \cdot \theta_1 + 2,65946 \cdot 10^{-2} \cdot \theta_2 + 1,25141 \\
 & \cdot \log(\text{Re}) + 1,96984 \cdot 10^{-1} \cdot \log\left(\frac{\varepsilon}{D_2}\right) + 1,97427 \cdot 10^{-3} \cdot \frac{H_1 H_2}{D_2 D_2} \\
 & - 3,38909 \cdot 10^{-3} \cdot \frac{H_1 R}{D_2 D_2} - 1,30213 \cdot 10^{-2} \cdot \frac{H_1 \theta_1}{D_2} + 1,04984 \\
 & \cdot 10^{-2} \cdot \frac{H_1 \theta_2}{D_2} + 1,84386 \cdot 10^{-2} \cdot \frac{H_1}{D_2} \cdot \log(\text{Re}) - 4,69650 \cdot 10^{-3} \\
 & \cdot \frac{H_1}{D_2} \cdot \log\left(\frac{\varepsilon}{D_2}\right) - 2,40159 \cdot 10^{-3} \cdot \frac{H_2 R}{D_2 D_2} - 2,14739 \cdot 10^{-3} \cdot \frac{H_2 \theta_1}{D_2} \\
 & - 2,86829 \cdot 10^{-3} \cdot \frac{H_2 \theta_2}{D_2} - 6,75587 \cdot 10^{-3} \cdot \frac{H_2}{D_2} \cdot \log(\text{Re}) \\
 & + 7,28020 \cdot 10^{-3} \cdot \frac{H_2}{D_2} \cdot \log\left(\frac{\varepsilon}{D_2}\right) - 3,10765 \cdot 10^{-3} \cdot \frac{R}{D_2} \cdot \theta_1 \\
 & + 6,25780 \cdot 10^{-3} \cdot \frac{R}{D_2} \cdot \theta_2 + 2,78799 \cdot 10^{-2} \cdot \frac{R}{D_2} \cdot \log(\text{Re}) \\
 & - 4,28271 \cdot 10^{-3} \cdot \frac{R}{D_2} \cdot \log\left(\frac{\varepsilon}{D_2}\right) + 2,72284 \cdot 10^{-3} \cdot \theta_1 \theta_2 \\
 & - 4,84578 \cdot 10^{-3} \cdot \theta_1 \cdot \log(\text{Re}) - 9,02891 \cdot 10^{-3} \cdot \theta_1 \cdot \log\left(\frac{\varepsilon}{D_2}\right) \\
 & - 1,05095 \cdot 10^{-2} \cdot \theta_2 \cdot \log(\text{Re}) - 8,86108 \cdot 10^{-3} \cdot \theta_2 \cdot \log\left(\frac{\varepsilon}{D_2}\right) \\
 & + 2,71011 \cdot 10^{-2} \cdot \log(\text{Re}) \cdot \log\left(\frac{\varepsilon}{D_2}\right) - 4,87378 \cdot 10^{-2} \cdot \left(\frac{H_1}{D_2}\right)^2 \\
 & - 9,02891 \cdot 10^{-4} \cdot \left(\frac{H_2}{D_2}\right)^2 - 1,05095 \cdot 10^{-2} \cdot \left(\frac{R}{D_2}\right)^2 - 8,86108 \\
 & \cdot 10^{-3} \cdot (\theta_1)^2 + 2,71011 \cdot 10^{-2} \cdot (\theta_2)^2 - 4,87378 \cdot 10^{-2} \\
 & \cdot (\log(\text{Re}))^2 + 4,80682 \cdot 10^{-4} \cdot \left(\log\left(\frac{\varepsilon}{D_2}\right)\right)^2
 \end{aligned} \tag{6}$$

REFERENCES

- [1] Lay CH, Sen B, Huang SC, Chen CC, Lin CY. Sustainable bioenergy production from tofu-processing wastewater by anaerobic hydrogen fermentation for onsite energy recovery. *Renew Energy* 2013;58:60–7.
- [2] Raabe J. *Hydro power: the design, use, and function of hydromechanical, hydraulic, and electrical equipment*. Düsseldorf: VDI-Verlag; 1985.
- [3] Akin H. Numerical methods development and implementation for hydraulic turbine design. MS thesis. Ankara, Turkey: TOBB University of Economics and Technology; December 2014.
- [4] Marquez JL, Molina MG, Pacas JM. Dynamic modeling, simulation and control design of an advanced micro-hydro power plant for distributed generation applications. *Int J Hydrogen Energy* 2010;35(11):5772–7.
- [5] Keck H, Sick M. Thirty years of numerical flow simulation in hydraulic turbomachines. *Acta Mech* 2008;201:211–29.
- [6] Hellström JGI, Marjavaara BD, Lundström TS. Parallel CFD simulations of an original and redesigned hydraulic turbine draft tube. *Adv Eng Softw* 2007;38(5):338–44.

- [7] Wu J, Shimmei K, Tani K, Niikura K, Sato J. CFD-based design optimization for hydro turbines. *J Fluids Eng* 2007;129(2):159–68.
- [8] McNabb J, Devals C, Kyriacou SA, Murry N, Mullins BF. CFD based draft tube hydraulic design optimization. In: *IOP Conference Series: Earth and Environmental Science*, Vol. 22. IOP Publishing; 2014 (1).
- [9] Georgopoulou C, Kyriacou S, Giannakoglou K, Grafenberger P, Parkinson E. Constrained multi-objective design optimization of hydraulic components using a hierarchical metamodel-assisted evolutionary algorithm. Part 1: Theory. In: *24th IAHR symposium on hydraulic machinery and systems*, Brazil; 2008.
- [10] Grafenberger P, Parkinson E, Georgopoulou C, Kyriacou S, Giannakoglou K. Constrained multi-objective design optimization of hydraulic components using a hierarchical metamodel-assisted evolutionary algorithm. Part 2: Applications. In: *24th IAHR symposium on hydraulic machinery and systems*, Brazil; 2008.
- [11] Ayancik F, Acar E, Celebioglu K, Aradag S. Simulation-based design and optimization of Francis turbine runners by using multiple types of metamodels, *Proceedings of the Institution of Mechanical Engineers, Part C. J Mech Eng Sci* 2016. <http://dx.doi.org/10.1177/0954406216658078>.
- [12] Arslan Y, Eken-Saracoglu N. Response surface optimization studies of the acid-catalysed hydrolysis of hazelnut shells. *Gazi Univ J Sci Part A Eng Innovation* 2015;3(No. 3):51–61.
- [13] Kieu HTQ, Nguyen YT, Dang YT, Nguyen BT. Use of response surface methodology to optimize culture conditions for hydrogen production by an anaerobic bacterial strain from soluble starch. *J Electron Mater* 2016;45(5):2632–8.
- [14] Fiordalis A, Georgakis C. Data-driven, using design of dynamic experiments, versus model-driven optimization of batch crystallization processes. *J Process Control* 2013;23(No. 2):179–88.
- [15] Acar E, Guler MA, Gerceker B, Cerit M, Karakaya E. Multi-objective crashworthiness optimization of tapered thin-walled tubes with axisymmetric indentations. *Thin-Walled Struct* 2011;49(1):94–105.
- [16] Krivchenko GI. *Hydraulic machines: turbines and pumps*. Moscow: Mir Publishers; 1986.
- [17] Gubin MF. *Draft tubes of hydroelectric stations*. New Delhi: Amerind Publishing Co. Pvt. Ltd.; 1973.
- [18] Aurora JS. *Introduction to optimum design*. 2nd ed. Elsevier, Academic Press; 2004.
- [19] Akin H, Aytac Z, Ayancik F, Ozkaya E, Arioz E, Celebioglu K, et al. A CFD aided hydraulic turbine design methodology applied to Francis turbines. In: *Power engineering, energy and electrical drives (POWERENG) 2013 fourth international conference on*. IEEE; May 2013. p. 694–9.
- [20] Ayli UE, Kaplan A, Cetinturk H, Kavurmaci B, Demirel G, Celebioglu K, et al. CFD analysis of 3D flow for 1.4 MW Francis turbine and model turbine manufacturing. In: *ASME 2015 international design engineering technical conferences and computers and information in engineering conference*. American Society of Mechanical Engineers; August 2015.
- [21] ANSYS design exploration user guide, release 14.5. October 2012.
- [22] Hothersall RJ. Assessing the design of draft tubes. *Int Water Power Dam Constr* 1988;40(4):55–7.
- [23] Seber GAF, Wild CJ. *Nonlinear regression*, Wiley series in probability and mathematical statistics. New York: Wiley; 1989.
- [24] Ozsaglam Y, Cunkas M. Particle swarm optimization algorithm for solving optimization problems. *J Polytech* 2008;11(4):299–305.
- [25] Ozsoy VS, Orkcü HH. Estimating the parameters of nonlinear regression models through particle swarm optimization. *Gazi Univ J Sci* 2016;29(1):187–99.